HHS Public Access

Author manuscript

Neuroimage. Author manuscript; available in PMC 2023 February 15.

Published in final edited form as:

Neuroimage. 2022 February 15; 247: 118727. doi:10.1016/j.neuroimage.2021.118727.

Insights into human cerebral white matter maturation and degeneration across the adult lifespan

Matthew Kiely, **Curtis Triebswetter**, **Luis E. Cortina**, **Zhaoyuan Gong**, **Maryam H. Alsameen**, **Richard G. Spencer**, **Mustapha Bouhrara***

Laboratory of Clinical Investigation, National Institute on Aging, National Institutes of Health, Baltimore, 21224 MD, USA

Abstract

White matter (WM) microstructural properties change across the adult lifespan and with neuronal diseases. Understanding microstructural changes due to aging is paramount to distinguish them from neuropathological changes. Conducted on a large cohort of 147 cognitively unimpaired subjects, spanning a wide age range of 21 to 94 years, our study evaluated sex- and age-related differences in WM microstructure. Specifically, we used diffusion tensor imaging (DTI) magnetic resonance imaging (MRI) indices, sensitive measures of myelin and axonal density, and myelin water fraction (MWF), a measure of the fraction of the signal of the water trapped within the myelin sheets, to probe these differences. Furthermore, we examined regional correlations between MWF and DTI indices to evaluate whether these metrics provide information complementary to MWF. While sexual dimorphism was, overall, nonsignificant, we observed region-dependent differences in MWF, that is, myelin content, and axonal density with age and found that both exhibit nonlinear, but distinct, associations with age. Furthermore, DTI indices were moderately correlated with MWF, indicating their good sensitivity to myelin content as well as to other constituents of WM tissue such as axonal density. The microstructural differences captured by our MRI metrics, along with their weak associations with MWF, strongly indicate the potential value of combining these outcome measures in a multiparametric approach. Furthermore, our results support the last-in-first-out and the gain-predicts-loss hypotheses of WM maturation and degeneration. Indeed, our results indicate that the posterior WM regions are spared from neurodegeneration as compared to anterior regions, while WM myelination follows a temporally symmetric time course across the adult life span.

*Corresponding author: Mustapha Bouhrara, PhD., Chief, Magnetic Resonance Physics of Aging and Dementia Unit, National Institute on Aging, National Institutes of Health, Intramural Research Program, BRC 05C-222, 251 Bayview Boulevard, Baltimore, MD, 21224, USA. Tel: 410-558-8541. bouhraram@mail.nih.gov.

Authors contribution

MB: experimental design and data acquisition, LC: data preprocessing, MK, CT, LC, ZG, MA, MB: data analysis, MK, CT, LC, ZG, MA, RS, MB: data interpretation, MK, MB: paper drafting, MK, CT, LEC, ZG, MA, RS, MB: paper editing.

Declaration of Competing Interest

The authors declare no financial competing interest.

Keywords

Myelin water fraction; Diffusion tensor imaging; Aging; Brain; Quantitative MRI

INTRODUCTION

Myelin loss and axonal damage of cerebral white matter (WM) have been associated with various neurological conditions such as Alzheimer's disease (AD), Parkinson's disease (PD), schizophrenia, multiple sclerosis, and traumatic brain injury (1–5). Characterizing the effect of normative aging on cerebral tissue integrity is fundamental to develop insights into normal physiology and distinguish it from neuropathology. Indeed, age is the main risk factor of neurodegeneration, leading to deficiencies in cognitive and motor functions, with more severe degeneration resulting in age-related diseases, including mild cognitive impairment (MCI) and dementias (4, 6–11). Although postmortem histological studies provide demonstrations of lifespan differences in cerebral microstructural integrity, including changes in myelin content and axonal density (10, 12), they are limited in their ability to perform correlative studies with cognitive outcomes or therapeutic interventions. Therefore, *in-vivo* characterization of differences in cerebral tissue microstructure with aging is paramount for identifying neuroimaging biomarkers of tissue status, distinguishing age-dependent changes from neuropathological changes, and evaluating treatments.

Previous studies have examined the effect of age on cerebral microstructure using, prominently, diffusion tensor imaging (DTI) indices such as fractional anisotropy (FA), mean diffusivity (MD), radial diffusivity (RD), and axial diffusivity (AxD); these magnetic resonance imaging (MRI) metrics have all been shown to represent sensitive probes of tissue microstructural integrity (13–22). However, results from these studies are sparse and conflicting, with some investigations indicating nonlinear trends of DTI-indices with age, while others have depicted linear or no trends (13, 17, 19, 23–25). Furthermore, although RD and FA are conventionally used as metrics to probe myelin content, the underlying structural mechanisms responsible for all DTI-indices are difficult to define due to their sensitivity to several tissue properties, including hydration, macromolecular content, axonal density, myelin content, and architectural features (26). Advanced relaxometry-based methods have been introduced to improve specificity of MR-based myelination studies through quantification of the myelin water fraction (MWF) (2, 27–50), and have been applied extensively to study the myelination patterns in diseases and neurodevelopment (1, 4, 31, 50–54). Although these investigations have provided pivotal insights into cerebral microstructural changes with aging and neuropathology, the literature regarding differences in MWF trends with age or sex remains limited and with conflicting results. Indeed, studies have found that MWF follows an inverted U-shaped trend with normative aging across different brain regions (19, 33, 55), indicating brain maturation until middle age, followed by a gradual process of demyelination, while others have found linear or no trends in MWF with advancing age (39, 56, 57). These results highlight the outstanding need for further advanced investigations on larger and well-characterized study cohorts.

Mounting evidence suggests that early maturating cerebral structures, such as the posterior regions, are spared from neurodegeneration as compared to the late maturating structures, such as the anterior regions; this is known as the retrogenesis paradigm (58, 59). In pioneering work, Bartzokis and colleagues postulate that, unlike heavily myelinated WM structures, late-myelinating WM structures are the earliest and most affected in AD, and concomitant damage to these fibers increases susceptibility to accumulation of amyloid-β and iron (60–64). The retrogenesis paradigm can be broken down into two main hypotheses, namely, the last-in-first-out hypothesis and the gain-predicts-loss hypothesis. The former suggests that slowly developing brain structures are the most vulnerable to neurodegeneration, while the latter hypothesis suggests that the maturation rate during neurodevelopment is equal to the rate of neurodegeneration at older ages. Therefore, knowledge of a tissue state in adulthood should predict the tissue state at a symmetric age after the peak. Emerging MRI evidence supports the retrogenesis paradigm (58, 65, 66). However, these investigations are still limited and were conducted using sensitive, but nonspecific, quantitative MRI techniques including relaxation times and DTI indices (19, 65, 66).

In this current work, we studied a large cohort of cognitively unimpaired subjects ($N = 147$) across the extended age range of 21–94 years. Our main objectives are to characterize age- and sex-related microstructural correlates by determining the DTI indices and MWF using our recently introduced method (34, 35, 67), within selected WM structures. We expect that combining different quantitative MR parameters will provide complementary information to dissociate the multiple biological processes involved in WM maturation and degeneration (19, 56, 68–71). Furthermore, we compared regional MWF estimates with widely used DTI indices of myelin content (FA, RD), axonal damage (AxD), and tissue composition (MD) to determine whether the information provided by these imaging biomarkers is complementary or redundant to MWF. We further evaluate whether a reduction in myelin content, as measured by MWF, could explain the age-related changes seen in some of these other parameters. Lastly, we sought to investigate the retrogenesis paradigm in this cohort of well-characterized cognitively unimpaired participants.

METHODS

Study cohort

Our study cohort consisted of cognitively unimpaired participants drawn from the Baltimore Longitudinal Study of Aging (BLSA) (72, 73), and the Genetic and Epigenetic Signatures of Translational Aging Laboratory Testing (GESTALT); two ongoing healthy aging cohorts at the National Institute on Aging to evaluate multiple biomarkers related to aging. The inclusion and exclusion criteria for these two studies are identical. Participants underwent a battery of cognitive tests and those with cognitive impairment were excluded (74). A detailed description of the cohort is presented in Table 1 and Figure 1. We note that age was not significantly different between men and women. Experimental procedures were performed in compliance with our local Institutional Review Board, and all subjects provided written informed consent.

MR imaging and parameters mapping

MRI experiments were performed on a 3T whole body Philips MRI system (Achieva, Best, The Netherlands) using the internal quadrature body coil for transmission and an eight-channel phased-array head coil for signal reception.

MWF determination—3D spoiled gradient recalled echo (SPGR) images were acquired with flip angles (FAs) of [2 4 6 8 10 12 14 16 18 20]°, echo time (TE) of 1.37 ms and repetition time (TR) of 5 ms, as well as 3D balanced steady state free precession (bSSFP) images acquired with FAs of [2 4 7 11 16 24 32 40 50 60]°, TE of 2.8 ms and TR of 5.8 ms. The bSSFP images were acquired with radiofrequency excitation pulse phase increments of 0 or π in order to account for off-resonance effects (75). All SPGR and bSSFP images were acquired with an acquisition matrix of 150 × 130 × 94, and voxel size of 1.6 mm × 1.6 mm × 1.6 mm. To correct for excitation radio frequency inhomogeneity, we used the double-angle method (DAM) (76) by acquiring two fast spin-echo images with FAs of 45° and 90°, TE of 102 ms, TR of 3000 ms, and acquisition voxel size of 2.6 mm × 2.6 mm × 4 mm. All images were acquired with field of view of 240 mm × 208 mm × 150 mm.

After thorough visual inspection of data quality for each participant, the scalp, ventricles and other nonparenchymal regions within the images were eliminated using the BET tool as implemented in the FSL software (77). Then, using the FLIRT tool of FSL (78), all SPGR, bSSFP and DAM images were linearly registered to the averaged SPGR image over FAs, and the derived transformation matrix was then applied to the original SPGR, bSSFP and DAM images. Next, a whole-brain MWF map was generated using the BMC-mcDESPOT analysis from the co-registered SPGR, bSSFP and DAM datasets (1, 34, 35, 67). Briefly, BMC-mcDESPOT assumes a two-component system consisting of a slowly relaxing and a more rapidly relaxing component. The rapidly relaxing component corresponds to the signal of water trapped within the myelin sheets while the slowly relaxing component corresponds to intra/extra cellular water. Analysis was performed explicitly accounting for nonzero TE as incorporated into the TE-corrected-mcDESPOT signal model (67).

DTI-indices determination—The DTI protocol consisted of diffusion-weighted images (DWI) acquired with single-shot EPI, TR of 10 s, TE of 70 ms, two *b*-values of 0 and 700 s/mm^2, with the latter encoded in 32 directions, acquisition matrix of 120 × 104 × 75, and acquisition voxel size of 2 mm × 2 mm × 2 mm. All images were acquired with field of view of 240 mm × 208 mm × 150 mm. The DW images were corrected for eddy current and motion effects using the affine registration tools as implemented in FSL (78), and registered to the DW image obtained with $b = 0$ s/mm^2 using FNIRT. We used the *DTIfit* tool implemented in FSL to calculate the eigenvalue maps which were used to calculate FA, RD, MD and AxD (79).

Parameter maps registration

As indicated above, the scalp, ventricles and other nonparenchymal regions within the images were eliminated using the BET tool as implemented in FSL (77). The SPGR image averaged over FAs for each participant was registered using nonlinear registration (FNIRT in FSL, with 12 degrees of freedom) to the Montreal Neurological Institute (MNI) standard

space image and the derived transformation matrix was then applied to the corresponding MWF map. Similarly, the DW image obtained at $b = 0$ s/mm^2 was nonlinearly registered to the MNI atlas and the calculated matrix of transformation was then applied to the corresponding FA, RD, MD, and AxD maps.

ROIs determination

Fourteen WM structures were chosen as regions-of-interest (ROIs) from the MNI atlas provided in FSL. These WM regions were defined from the Johns Hopkins University (JHU) ICM-DTI-81 atlas encompassing the whole brain (WB) WM, frontal (FL), occipital (OL), parietal (PL) and temporal (TL) lobes WM, cerebellum (CRB) WM, corpus callosum (CC), internal capsule (IC), cerebral peduncle (CP), corona radiata (CR), thalamic radiation (TR), fronto-occipital fasciculus (FOF), longitudinal fasciculus (LF), and forceps (FO). All ROIs were eroded to reduce partial volume effects and imperfect image registration, and to mitigate structural atrophy seen especially at older ages. For each ROI and participant, the mean MWF, FA, MD, RD and AxD values were calculated.

Statistical analyses

In this study, we conducted four different analyses:

1. *Effects of age and sex on MWF and DTI-indices*: the goal of this analysis was to investigate age and sex effects on MWF, RD, FA, MD, and AxD. For each ROI, a multiple linear regression model was evaluated using the mean ROI values for MWF, FA, MD, RD or AxD as the dependent variable and sex and age as the independent variables. We incorporated a quadratic age term, age^2, after mean age centering, in the regression model given by:

$$\mathrm{P}_i = \beta_0 + \beta_{sex} \times \mathrm{sex}_i + \beta_{age} \times \mathrm{age}_i + \beta_{age}2 \times \mathrm{age}_i 2,$$

where P_i is the mean ROI value of the parameter of interest (*i.e.*, MWF, FA, MD, RD, or AxD) of participant *i*. This analysis was conducted using the *fitlm* function as implemented in the MATLAB software.

Furthermore, for each ROI and each parameter, we performed a likelihood-ratio test for the regression models with and without a quadratic age term to assess whether the data supports a linear model or a quadratic model.

2. *Correlation analysis between MWF and DTI indices*: it has been widely assumed that the DTI outcomes, especially FA and RD, could serve as specific metrics to probe differences in myelin content with neurodevelopment or neuropathology (80–82). Here, for each ROI, we tested this assumption using Pearson correlation by correlating each derived DTI parameter, that is, FA, MD, RD or AxD to MWF, which represents a more specific measure of myelin content (2, 83, 84).

3. *The last-in-first-out hypothesis*: the retrogenesis paradigm suggests that the early maturating cerebral structures, that is, the posterior regions, are spared from neurodegeneration as compared to the late maturating structures, that is, the

anterior regions. To test this, we calculated the age at the maximum or minimum, as appropriate, of the parameter under consideration for each ROI.

4. *The gain-predicts-loss hypothesis*: the gain-predicts-loss hypothesis suggests that the rate of tissue gain during maturation at younger age will equal the rate of tissue loss during degeneration at older age (65). Therefore, knowledge of a tissue state in early adulthood should predict the tissue state at a symmetric age post peak. To test this paradigm, we characterized the lifespan changes in MWF and DTI indices for each ROI by fitting the data to a piecewise linear model as described previously (60). For each ROI, a piecewise linear model consisting of two segments was developed, with the first corresponding to maturation and the second to degeneration. The point of transition was defined as the maximum or minimum, as appropriate, of the parameter under consideration. The slopes of these two segments defined the rates of maturation and degeneration; their absolute values were compared statistically for each ROI investigated (85).

For each analysis, the threshold for statistical significance was taken as $p < 0.05$ after correction for multiple ROI comparisons using the false discovery rate (FDR) method (86, 87). All analyses were run using MATLAB software.

RESULTS

Age and sex effects on MWF and DTI indices

Figure 2 illustrates the regional differences in MWF and DTI indices maps across the adult lifespan, demonstrated using one representative slice from averaged brain maps from participants within each age decade. The parameter maps exhibit tissue contrast between different brain substructures and across age decades. Visual inspection suggests regional increases in MWF from early adulthood until middle age, 40–59 years, followed by decreases in MWF at older ages. In contrast, visual inspection of FA maps suggests, overall, regional decreases with age while MD, RD and AxD maps suggest, overall, regional increases with age within most brain regions.

Figure 3 shows the MWF and DTI indices as a function of age for 5 representative WM regions investigated. Visual inspection indicates that MWF and FA generally increase until middle age, followed by a decline with advanced age. Conversely, MD, RD and AxD generally decrease until middle age, followed by an increase afterwards. The best-fit curves indicate that while the fundamental nonlinear relationship between MWF or DTI indices and age was consistent across all ROIs, the age curves displayed regional variation, as expected. Furthermore, our statistical analysis revealed significant age effects on MWF and DTI indices for most cerebral structures studied (Table 2). Similarly, the quadratic effect of age, that is, age^2, on all investigated parameters was significant in most ROIs. The *p*-values associated with this statistical analysis are shown in our Supplementary Materials (Table S1). To further support our choice of model, we applied the likelihood-ratio test to determine whether the model incorporating a quadratic age term better described the data. For all ROIs and each MR parameter, the likelihood-ratio test indicated that the model incorporating a quadratic age term provided significantly better fit to the data in all ROIs investigated,

expect the CP and LF structures for FA (Table 3). Finally, the sex effect was limited to a very few structures for all metrics. Additional plots representing each ROI in detail are found in our Supplementary Material (Figs. S1–S5).

Regional correlations between MWF and DTI indices

Correlations between MWF and DTI indices are shown in Figure 4. Pearson correlations across 12 of the 14 ROIs demonstrate significant correlations, while the cerebellum (FA, MD, or AxD *vs.* MWF) and cerebral peduncle (all DTI indices *vs.* MWF) exhibited no significance. Figure 5 shows the direction of these trends: FA *vs.* MWF exhibited significant positive correlations, while RD *vs.* MWF, MD *vs.* MWF, and AxD *vs.* MWF exhibited significant negative correlations, as expected. However, in terms of effect size, all DTI indices exhibited weak-to-moderate correlations with MWF, with RD exhibiting, overall, the highest coefficient of correlation with MWF. Additional plots representing each ROI in detail are found in our supplementary material (Supplementary Figs. S6–S9).

Last-in-first-out paradigm

Table 4 shows, for each ROI, the calculated specific year at which MWF or DTI indices peaked, when applicable. This was used to investigate the last-in-first-out hypothesis by comparing the age of maximum maturation between the posterior and anterior regions of the brain. As seen, DTI indices peaked earlier as compared to MWF for most ROIs in agreement with Figs. 2–3. Furthermore, the MWF and DTI indices of the posterior brain regions, especially, the occipital and temporal lobes as well as the cerebellum reached a peak age at later ages as compared to all other cerebral structures including the anterior structures such as the frontal lobes.

Gain-predicts-lost paradigm

The gain-predicts-loss hypothesis was then investigated, in each ROI and for each MR metric, through calculation and comparison of the maturation and degeneration rates. Figure 6 provides a comparison of the maturation and degeneration phases as a function of age for 5 representative WM regions and each MR parameter studied. Visual inspection indicates that the maturation and degeneration rates are near-symmetrical especially for MWF but only in a few ROIs for the diffusivity indices. Table 5 shows the calculated rates with corresponding standard errors (SEs). For each metric and each ROI, the absolute magnitudes of the maturation and degeneration rates were statistically compared. The results indicate no statistical differences between the magnitudes of maturation and degeneration rates. Additional plots representing each ROI in detail are found in our supplementary material (Supplementary Figs. S10–S14). Further, for all parameters and ROIs, the SEs of the maturation rates were much higher than those of the degeneration rates. Additionally, the SEs of the rates of the DTI indices were much higher than those of the rates of the MWF metric.

DISCUSSION

We used advanced quantitative MRI parameters, namely, MWF and DTI indices, to characterize the maturation and degeneration phases of the human cerebrum across the adult

lifespan in a large cohort of well-characterized cognitively unimpaired subjects spanning a wide age range. Our goal was to establish specific and sensitive *in-vivo* imaging biomarkers that can help define the evolution of normal aging in the cerebrum and characterize the heterogenous regional alterations that reflect the microstructural status of white matter tissue. We believe that the present work provides a unique description of MR neuroimaging biomarkers in the human brain by incorporating a large cohort of cognitively normal adults and an exhaustive number of quantitative MR measures. These MR markers offer the possibility of probing tissue biophysical properties and may help to further define the relationships between changes in cognition, function, and tissue microstructure.

Our results demonstrate strong regional quadratic trends of our MR measures with age, peaking at approximately middle age. The quadratic association between MWF and age in white matter regions observed in the present study (N = 147, 21–94 years), conducted on the largest cohort size with the widest adult age range and improved age distribution to date, is consistent with our previous report (N = 106, 22–94 years), Arshad and colleagues' study (N = 61, 18–84 years) and Dvorak and colleagues' recent study (N = 100, 20–78 years), all describe an inverted U-shape trend of MWF values with age in different white matter regions (19, 33, 55). This quadratic association is attributed to the process of myelination from youth through middle age, followed by demyelination in later years (19, 33, 55, 63); this pattern is in agreement with postmortem observations (10, 12). As expected, we found that different regions exhibit both similarities and differences in associations between MWF and age, with most regions peaking at the fifth decade of life. However, and surprisingly, Billiet's study (N = 59, 17–70 years) showed no difference in MWF with age, while Canales-Rodríguez and colleagues (N = 145, 18–60 years) observed linear regional trends between MWF and age (56, 57). However, the age range of the cohorts in these studies was relatively limited. Indeed, although Billiet's study incorporated a wide age range, it did not include subjects above the age of 70 and incorporates only three subjects over 60 years, while Canales-Rodríguez's cohort was composed primarily of relatively young adult subjects. These limitations in previous studies may have precluded detection of the nonlinear, more biologically plausible, association of MWF with age. Indeed, nonlinear patterns with age in various WM brain structures have been found using conventional quantitative MRI methods, including DTI indices (13, 19, 61, 65, 88–90). Our DTI results are consistent with these reports, indicating a U-shaped relationship between the diffusivity metrics and age in most ROIs, with FA exhibiting an inverted U-shaped relationship. These results further support the notion of white matter maturation until middle age followed by a phase of degeneration. However, interestingly, all DTI indices peaked at earlier ages as compared to MWF, in agreement with previous reports (17, 24, 89); this highlights that DTI indices are sensitive to the underlying microarchitectural status of the brain parenchyma and the degree and direction of water molecule mobility, yielding information complementary to MWF. Indeed, our results indicate that all DTI indices exhibited weak-to-moderate correlations with MWF. This supports the notion that these DTI indices, including FA and RD, cannot serve as specific markers of myelin content due to their sensitivity to other microstructural characteristics including axonal density (19, 56, 69, 91). Therefore, any of these diffusion parameters alone cannot describe the temporal and spatial maturation and degeneration processes involved in senescence, highlighting the value of using multiple

advanced and conventional quantitative MRI metrics that are specific or sensitive to distinct tissue features for clinical research (92–94).

Our quantitative analyses showed that the occipital lobes exhibited delayed maturation compared to the other lobes. This pattern is consistent with the last-in-first-out paradigm, in which posterior brain regions are spared from degeneration in contrast to anterior brain regions (58, 59, 95–97). However, additional studies, particularly longitudinal studies, are required for further validation. Finally, we tested the gain-predicts-loss hypothesis in the specific context of brain maturation and degeneration. Using longitudinal relaxation rate and diffusion metrics, previous MRI-based studies have demonstrated support for this theory in the cerebrum (66, 98), and have indicated that age-related processes are, to a certain extent, mirror-symmetric developmental processes in terms of time-course. In agreement with these observations, our novel results, especially using MWF mapping, provide support to the gain-predicts-loss hypothesis of tissue maturation and degeneration in the white matter tissue. Indeed, MWF followed regional curve shapes that were roughly symmetric with respect to age in most regions evaluated. We interpret these results as indicating that maturation and degeneration of myelin sheets occur in a more temporally symmetric fashion. If confirmed, the MWF model will guide early interventions as it suggests that knowledge of a tissue state in early adulthood should predict the tissue state at a symmetric age post peak. Interestingly, this was, overall, not the case for the DTI indices for which the degenerative phase occurred more rapidly than the maturation phase. The DTI indices, as indicated above, reached the maximum maturation at earlier ages when compared to MWF. Therefore, assessing the gain-predicts-loss paradigm in this context is unreliable given the limited data points in the maturation phase, as reflected by the large SEs in derived rates. Histological analyses, longitudinal studies, and studies involving younger participants are required to confirm our findings.

Although conducted on a large cohort and using state-of-the-art methods, our investigation has limitations. Our cohort does not include very young participants (< 20 years old); inclusion of younger participants may influence the quantification of the age trends (99) as well as the interpretation of the symmetrical trends observed between the maturation and degeneration phases. Moreover, contamination due to partial volume issues may have been introduced in the calculated MWF and DTI indices derived values. To minimize this potential effect, all ROIs were eroded followed by careful visual inspection. Nevertheless, some partial volume effects could have persisted, especially in small structures. In addition, age-related tissue atrophy could lead to non-optimal image registration, potentially introducing some bias in derived parameter values. Nevertheless, visual inspection indicates that age-related tissue atrophy was limited to a very few participants belonging to the oldest age decade of our cohort. Finally, several physiological and experimental parameters could bias MWF determination. These include, but are not limited to, exchange between water pools (100–102), magnetization transfer between free water protons and macromolecules (100, 103), iron content (104), internal gradients (105, 106) and differential signal attenuation due to water diffusion in underlying compartments (107–109), which are not considered in either the BMC-mcDESPOT formalism or the other MWF measurement methods available. However, the multi-spin-echo (MSE)-based MRI sequences remain the reference methods for MWF mapping (2, 45, 83, 110–112). This is likely due to the

availability of these imaging sequences on most preclinical and clinical MRI systems, the simplicity of the signal model, and the extensive histological validation conducted over the last two decades (28, 29). However, it must be emphasized that, although validated with histology, MWF corresponds to the ratio of the short relaxing component fraction, presumably attributed to the myelin water signal, to the total water. Therefore, this measure could be biased in the case of a substantial increase in the extra-cellular water due to edema or inflammation. Finally, further histological-based validation of the MWF estimates derived using BMC-mcDESPOT is required.

CONCLUSIONS

On a uniquely large cohort of cognitively normal adults spanning a wide age range and using MWF and DTI MRI measures, we confirmed that brain maturation continues until middle age followed by a phase of rapid degeneration at older ages. Sexual dimorphism in all these parameters was, overall, not significant. Furthermore, weak-to-moderate correlations between the DTI indices and MWF were observed, indicating the potential of using these outcome measures in a multiparametric approach in clinical investigations. Finally, our novel results support the last-in-first-out and the gain-predicts-loss hypotheses of cerebral white matter maturation and degeneration.

Supplementary Material

Refer to Web version on PubMed Central for supplementary material.

Acknowledgements

This work was supported by the Intramural Research Program of the National Institute on Aging of the National Institutes of Health.

References

1. Bouhrara M, Reiter D, Bergeron C, Zukley L, Ferrucci L, Resnick S, et al. Evidence of demyelination in mild cognitive impairment and dementia using a direct and specific magnetic resonance imaging measure of myelin content. Alzheimer's & Dementia. 2018;14(8):998–1004.
2. MacKay AL, Laule C. Magnetic Resonance of Myelin Water: An in vivo Marker for Myelin. Brain Plasticity. 2016;2(1):71–91. [PubMed: 29765849]
3. Dean DC III, Sojkova J, Hurley S, Kecskemeti S, Okonkwo O, Bendlin BB, et al. Alterations of Myelin Content in Parkinson's Disease: A Cross-Sectional Neuroimaging Study. PLOS ONE. 2016;11(10):e0163774. [PubMed: 27706215]
4. Flynn SW, Lang DJ, Mackay AL, Goghari V, Vavasour IM, Whittall KP, et al. Abnormalities of myelination in schizophrenia detected in vivo with MRI, and post-mortem with analysis of oligodendrocyte proteins. Molecular psychiatry. 2003;8(9):811–20. [PubMed: 12931208]
5. Benjamini D, Iacono D, Komlosh ME, Perl DP, Brody DL, Basser PJ. Diffuse axonal injury has a characteristic multidimensional MRI signature in the human brain. Brain. 2021;144(3):800–16. [PubMed: 33739417]
6. Kolasinski J, Stagg CJ, Chance SA, Deluca GC, Esiri MM, Chang E-H, et al. A combined post-mortem magnetic resonance imaging and quantitative histological study of multiple sclerosis pathology. Brain : a journal of neurology. 2012;135(Pt 10):2938–51. [PubMed: 23065787]
7. Bronge L, Bogdanovic N, Wahlund LO. Postmortem MRI and Histopathology of White Matter Changes in Alzheimer Brains. Dementia and Geriatric Cognitive Disorders. 2002;13(4):205–12. [PubMed: 12006730]

8. Pannese E Morphological changes in nerve cells during normal aging. Brain Struct Funct. 2011;216(2):85–9. [PubMed: 21431333]
9. Stassart RM, Möbius W, Nave K-A, Edgar JM. The Axon-Myelin Unit in Development and Degenerative Disease. Frontiers in Neuroscience. 2018;12(467).
10. Tang Y, Nyengaard JR, Pakkenberg B, Gundersen HJ. Age-induced white matter changes in the human brain: a stereological investigation. Neurobiology of aging. 1997;18(6):609–15. [PubMed: 9461058]
11. Marner L, Nyengaard JR, Tang Y, Pakkenberg B. Marked loss of myelinated nerve fibers in the human brain with age. J Comp Neurol. 2003;462(2):144–52. [PubMed: 12794739]
12. Peters A The effects of normal aging on myelin and nerve fibers: a review. Journal of neurocytology. 2002;31(8–9):581–93. [PubMed: 14501200]
13. Fjell AM, Engvig A, Tamnes CK, Grydeland H, Walhovd KB, Westlye LT, et al. Life-Span Changes of the Human Brain White Matter: Diffusion Tensor Imaging (DTI) and Volumetry. Cerebral Cortex. 2009;20(9):2055–68. [PubMed: 20032062]
14. Honea RA, Vidoni E, Harsha A, Burns JM. Impact of APOE on the healthy aging brain: a voxel-based MRI and DTI study. J Alzheimers Dis. 2009;18(3):553–64. [PubMed: 19584447]
15. Kodiweera C, Alexander AL, Harezlak J, McAllister TW, Wu Y-C. Age effects and sex differences in human brain white matter of young to middle-aged adults: A DTI, NODDI, and q-space study. NeuroImage. 2016;128:180–92. [PubMed: 26724777]
16. Oishi K, Mielke MM, Albert M, Lyketsos CG, Mori S. DTI analyses and clinical applications in Alzheimer's disease. J Alzheimers Dis. 2011;26 Suppl 3:287–96. [PubMed: 21971468]
17. Westlye LT, Walhovd KB, Dale AM, Bjørnerud A, Due-Tønnessen P, Engvig A, et al. Life-span changes of the human brain white matter: diffusion tensor imaging (DTI) and volumetry. Cereb Cortex. 2010;20(9):2055–68. [PubMed: 20032062]
18. Arfanakis K, Gui M, Tamhane AA, Carew JD. Investigating the Medial Temporal Lobe in Alzheimer's Disease and Mild Cognitive Impairment, with Turboprop Diffusion Tensor Imaging, MRI-volumetry, and T 2-relaxometry. Brain Imaging and Behavior. 2007;1(1):11–21.
19. Arshad M, Stanley JA, Raz N. Adult age differences in subcortical myelin content are consistent with protracted myelination and unrelated to diffusion tensor imaging indices. NeuroImage. 2016;143:26–39. [PubMed: 27561713]
20. Bozzali M, Falini A, Franceschi M, Cercignani M, Zuffi M, Scotti G, et al. White matter damage in Alzheimer's disease assessed in vivo using diffusion tensor magnetic resonance imaging. Journal of Neurology, Neurosurgery & Psychiatry. 2002;72(6):742–6.
21. Menzler K, Belke M, Wehrmann E, Krakow K, Lengler U, Jansen A, et al. Men and women are different: diffusion tensor imaging reveals sexual dimorphism in the microstructure of the thalamus, corpus callosum and cingulum. NeuroImage. 2011;54(4):2557–62. [PubMed: 21087671]
22. Alisch JSR, Kiely M, Triebswetter C, Alsameen MH, Gong Z, Khattar N, et al. Characterization of Age-Related Differences in the Human Choroid Plexus Volume, Microstructural Integrity, and Blood Perfusion Using Multiparameter Magnetic Resonance Imaging. Frontiers in Aging Neuroscience. 2021;13(613).
23. Cox SR, Ritchie SJ, Tucker-Drob EM, Liewald DC, Hagenaars SP, Davies G, et al. Ageing and brain white matter structure in 3,513 UK Biobank participants. Nature Communications. 2016;7(1):13629.
24. Lebel C, Beaulieu C. Longitudinal Development of Human Brain Wiring Continues from Childhood into Adulthood. The Journal of Neuroscience. 2011;31(30):10937–47. [PubMed: 21795544]
25. Bouhrara M, Cortina LE, Khattar N, Rejimon AC, Ajamu S, Cezayirli DS, et al. Maturation and degeneration of the human brainstem across the adult lifespan. Aging. 2021;13(11):14862–91. [PubMed: 34115614]
26. Wheeler-Kingshott CAM, Cercignani M. About "axial" and "radial" diffusivities. Magnetic resonance in medicine. 2009;61(5):1255–60. [PubMed: 19253405]
27. MacKay A, Whittall K, Adler J, Li D, Paty D, Graeb D. In vivo visualization of myelin water in brain by magnetic resonance. Magnetic resonance in medicine. 1994;31(6):673–7. [PubMed: 8057820]

28. Laule C, Kozlowski P, Leung E, Li DK, Mackay AL, Moore GR. Myelin water imaging of multiple sclerosis at 7 T: correlations with histopathology. NeuroImage. 2008;40(4):1575–80. [PubMed: 18321730]
29. Laule C, Leung E, Lis DK, Traboulsee AL, Paty DW, MacKay AL, et al. Myelin water imaging in multiple sclerosis: quantitative correlations with histopathology. Multiple sclerosis (Houndmills, Basingstoke, England). 2006;12(6):747–53.
30. Björk M, Zachariah D, Kullberg J, Stoica P. A multicomponent T2 relaxometry algorithm for myelin water imaging of the brain. Magnetic resonance in medicine. 2016;75(1):390–402. [PubMed: 25604436]
31. Borich MR, MacKay AL, Vavasour IM, Rauscher A, Boyd LA. Evaluation of white matter myelin water fraction in chronic stroke. NeuroImage: Clinical. 2013;2:569–80. [PubMed: 24179808]
32. Bouhrara M, Reiter DA, Maring MC, Bonny JM, Spencer RG. Use of the NESMA Filter to Improve Myelin Water Fraction Mapping with Brain MRI. J Neuroimaging. 2018;28(6):640–9. [PubMed: 29999204]
33. Bouhrara M, Rejimon AC, Cortina LE, Khattar N, Bergeron CM, Ferrucci L, et al. Adult brain aging investigated using BMC-mcDESPOT based myelin water fraction imaging. Neurobiology of aging. 2020;85:131–9. [PubMed: 31735379]
34. Bouhrara M, Spencer RG. Improved determination of the myelin water fraction in human brain using magnetic resonance imaging through Bayesian analysis of mcDESPOT. NeuroImage. 2016;127:456–71. [PubMed: 26499810]
35. Bouhrara M, Spencer RG. Rapid simultaneous high-resolution mapping of myelin water fraction and relaxation times in human brain using BMC-mcDESPOT. NeuroImage. 2017;147:800–11. [PubMed: 27729276]
36. Dean DC 3rd, O'Muircheartaigh J, Dirks H, Waskiewicz N, Lehman K, Walker L, et al. Estimating the age of healthy infants from quantitative myelin water fraction maps. Human brain mapping. 2015;36(4):1233–44. [PubMed: 25640476]
37. Deoni SC, Kolind SH. Investigating the stability of mcDESPOT myelin water fraction values derived using a stochastic region contraction approach. Magnetic resonance in medicine. 2015;73(1):161–9. [PubMed: 24464472]
38. Deoni SCL, Dean DC, O'Muircheartaigh J, Dirks H, Jerskey BA. Investigating white matter development in infancy and early childhood using myelin water faction and relaxation time mapping. NeuroImage. 2012;63(3):1038–53. [PubMed: 22884937]
39. Faizy TD, Kumar D, Broocks G, Thaler C, Flottmann F, Leischner H, et al. Age-Related Measurements of the Myelin Water Fraction derived from 3D multi-echo GRASE reflect Myelin Content of the Cerebral White Matter. Scientific Reports. 2018;8(1):14991. [PubMed: 30301904]
40. Faizy TD, Thaler C, Kumar D, Sedlacik J, Broocks G, Grosser M, et al. Heterogeneity of Multiple Sclerosis Lesions in Multislice Myelin Water Imaging. PLoS One. 2016;11(3):e0151496. [PubMed: 26990645]
41. Guo J, Ji Q, Reddick WE. Multi-slice Myelin Water Imaging for Practical Clinical Applications at 3.0 T. Magnetic resonance in medicine : official journal of the Society of Magnetic Resonance in Medicine / Society of Magnetic Resonance in Medicine. 2013;70(3):813–22.
42. Hwang D, Chung H, Nam Y, Du YP, Jang U. Robust mapping of the myelin water fraction in the presence of noise: synergic combination of anisotropic diffusion filter and spatially regularized nonnegative least squares algorithm. Journal of magnetic resonance imaging : JMRI. 2011;34(1):189–95. [PubMed: 21618330]
43. Hwang D, Kim DH, Du YP. In vivo multi-slice mapping of myelin water content using T2* decay. NeuroImage. 2010;52(1):198–204. [PubMed: 20398770]
44. Kolind S, Matthews L, Johansen-Berg H, Leite MI, Williams SC, Deoni S, et al. Myelin water imaging reflects clinical variability in multiple sclerosis. NeuroImage. 2012;60(1):263–70. [PubMed: 22155325]
45. Lee J, Hyun J-W, Lee J, Choi E-J, Shin H-G, Min K, et al. So You Want to Image Myelin Using MRI: An Overview and Practical Guide for Myelin Water Imaging. Journal of Magnetic Resonance Imaging. 2021;53(2):360–73. [PubMed: 32009271]

46. Lenz C, Klarhofer M, Scheffler K. Feasibility of in vivo myelin water imaging using 3D multigradient-echo pulse sequences. Magnetic resonance in medicine. 2012;68(2):523–8. [PubMed: 22213038]
47. Nam Y, Lee J, Hwang D, Kim DH. Improved estimation of myelin water fraction using complex model fitting. NeuroImage. 2015;116:214–21. [PubMed: 25858448]
48. Prasloski T, Rauscher A, MacKay AL, Hodgson M, Vavasour IM, Laule C, et al. Rapid whole cerebrum myelin water imaging using a 3D GRASE sequence. NeuroImage. 2012;63(1):533–9. [PubMed: 22776448]
49. Shin HG, Oh SH, Fukunaga M, Nam Y, Lee D, Jung W, et al. Advances in gradient echo myelin water imaging at 3T and 7T. NeuroImage. 2018.
50. Sirrs SM, Laule C, Madler B, Brief EE, Tahir SA, Bishop C, et al. Normal-appearing white matter in patients with phenylketonuria: water content, myelin water fraction, and metabolite concentrations. Radiology. 2007;242(1):236–43. [PubMed: 17185670]
51. Laule C, Vavasour IM, Moore GR, Oger J, Li DK, Paty DW, et al. Water content and myelin water fraction in multiple sclerosis. A T2 relaxation study. Journal of neurology. 2004;251(3):284–93. [PubMed: 15015007]
52. Dean DC 3rd, Hurley SA, Kecskemeti SR, O'Grady JP, Canda C, Davenport-Sis NJ, et al. Association of Amyloid Pathology With Myelin Alteration in Preclinical Alzheimer Disease. JAMA neurology. 2017;74(1):41–9. [PubMed: 27842175]
53. Bouhrara M, Reiter DA, Spencer RG. Bayesian analysis of transverse signal decay with application to human brain. Magnetic resonance in medicine. 2015;74(3):785–802. [PubMed: 25242062]
54. Bouhrara M, Cortina LE, Rejimon AC, Khattar N, Bergeron C, Bergeron J, et al. Quantitative age-dependent differences in human brainstem myelination assessed using high-resolution magnetic resonance mapping. NeuroImage. 2020;206:116307. [PubMed: 31669302]
55. Dvorak AV, Swift-LaPointe T, Vavasour IM, Lee LE, Abel S, Russell-Schulz B, et al. An atlas for human brain myelin content throughout the adult life span. Sci Rep. 2021;11(1):269. [PubMed: 33431990]
56. Billiet T, Vandenbulcke M, Mädler B, Peeters R, Dhollander T, Zhang H, et al. Age-related microstructural differences quantified using myelin water imaging and advanced diffusion MRI. Neurobiology of aging. 2015;36(6):2107–21. [PubMed: 25840837]
57. Canales-Rodríguez EJ, Alonso-Lana S, Verdolini N, Sarró S, Feria I, Montoro I, et al. Age- and gender-related differences in brain tissue microstructure revealed by multi-component T2 relaxometry. Neurobiology of aging. 2021.
58. Brickman AM, Meier IB, Korgaonkar MS, Provenzano FA, Grieve SM, Siedlecki KL, et al. Testing the white matter retrogenesis hypothesis of cognitive aging. Neurobiology of aging. 2012;33(8):1699–715. [PubMed: 21783280]
59. Raz N Aging of the brain and its impact on cognitive performance: Integration of structural and functional findings. The handbook of aging and cognition, 2nd ed. Mahwah, NJ, US: Lawrence Erlbaum Associates Publishers; 2000. p. 1–90.
60. Bartzokis G Age-related myelin breakdown: a developmental model of cognitive decline and Alzheimer's disease. Neurobiology of aging. 2004;25(1):5–18; author reply 49–62. [PubMed: 14675724]
61. Bartzokis G, Cummings JL, Sultzer D, Henderson VW, Nuechterlein KH, Mintz J. White Matter Structural Integrity in Healthy Aging Adults and Patients With Alzheimer Disease: A Magnetic Resonance Imaging Study. Archives of Neurology. 2003;60(3):393–8. [PubMed: 12633151]
62. Bartzokis G, Lu PH, Mintz J. Human brain myelination and amyloid beta deposition in Alzheimer's disease. Alzheimer's & dementia : the journal of the Alzheimer's Association. 2007;3(2):122–5.
63. Bartzokis G, Lu PH, Tingus K, Mendez MF, Richard A, Peters DG, et al. Lifespan trajectory of myelin integrity and maximum motor speed. Neurobiology of aging. 2010;31(9):1554–62. [PubMed: 18926601]
64. Khattar N, Triebswetter C, Kiely M, Ferrucci L, Resnick SM, Spencer RG, et al. Investigation of the association between cerebral iron content and myelin content in normative aging

using quantitative magnetic resonance neuroimaging. NeuroImage. 2021;239:118267. [PubMed: 34139358]

65. Yeatman JD, Wandell BA, Mezer AA. Lifespan maturation and degeneration of human brain white matter. Nature communications. 2014;5:4932-.
66. Slater DA, Melie-Garcia L, Preisig M, Kherif F, Lutti A, Draganski B. Evolution of white matter tract microstructure across the life span. Human brain mapping. 2019;40(7):2252–68. [PubMed: 30673158]
67. Bouhrara M, Spencer RG. Incorporation of nonzero echo times in the SPGR and bSSFP signal models used in mcDESPOT. Magnetic resonance in medicine. 2015;74(5):1227–35. [PubMed: 26407635]
68. Lambert C, Chowdhury R, Fitzgerald THB, Fleming SM, Lutti A, Hutton C, et al. Characterizing aging in the human brainstem using quantitative multimodal MRI analysis. Frontiers in human neuroscience. 2013;7:462-. [PubMed: 23970860]
69. Faizy TD, Thaler C, Broocks G, Flottmann F, Leischner H, Kniep H, et al. The Myelin Water Fraction Serves as a Marker for Age-Related Myelin Alterations in the Cerebral White Matter – A Multiparametric MRI Aging Study. Frontiers in Neuroscience. 2020;14(136).
70. Uddin MN, Figley TD, Solar KG, Shatil AS, Figley CR. Comparisons between multi-component myelin water fraction, T1w/T2w ratio, and diffusion tensor imaging measures in healthy human brain structures. Scientific Reports. 2019;9(1):2500. [PubMed: 30792440]
71. Callaghan MF, Freund P, Draganski B, Anderson E, Cappelletti M, Chowdhury R, et al. Widespread age-related differences in the human brain microstructure revealed by quantitative magnetic resonance imaging. Neurobiology of aging. 2014;35(8):1862–72. [PubMed: 24656835]
72. Shock N Normal Human Aging: The Baltimore Longitudinal Study of Aging. Journal of Gerontology. 1985;40(6):767–74.
73. Ferrucci L The Baltimore Longitudinal Study of Aging (BLSA): a 50-year-long journey and plans for the future. The journals of gerontology Series A, Biological sciences and medical sciences. 2008;63(12):1416–9.
74. O'Brien RJ, Resnick SM, Zonderman AB, Ferrucci L, Crain BJ, Pletnikova O, et al. Neuropathologic studies of the Baltimore Longitudinal Study of Aging (BLSA). Journal of Alzheimer's disease : JAD. 2009;18(3):665–75. [PubMed: 19661626]
75. Deoni SC. Correction of main and transmit magnetic field (B0 and B1) inhomogeneity effects in multicomponent-driven equilibrium single-pulse observation of T1 and T2. Magnetic resonance in medicine. 2011;65(4):1021–35. [PubMed: 21413066]
76. Stollberger R, Wach P. Imaging of the active B1 field in vivo. Magnetic resonance in medicine. 1996;35(2):246–51. [PubMed: 8622590]
77. Smith SM. Fast robust automated brain extraction. Human brain mapping. 2002;17(3):143–55. [PubMed: 12391568]
78. Jenkinson M, Beckmann CF, Behrens TE, Woolrich MW, Smith SM. FSL. NeuroImage. 2012;62(2):782–90. [PubMed: 21979382]
79. Basser PJ, Jones DK. Diffusion-tensor MRI: theory, experimental design and data analysis - a technical review. NMR in biomedicine. 2002;15(7–8):456–67. [PubMed: 12489095]
80. Janve VA, Zu Z, Yao SY, Li K, Zhang FL, Wilson KJ, et al. The radial diffusivity and magnetization transfer pool size ratio are sensitive markers for demyelination in a rat model of type III multiple sclerosis (MS) lesions. NeuroImage. 2013;74:298–305. [PubMed: 23481461]
81. Song S-K, Yoshino J, Le TQ, Lin S-J, Sun S-W, Cross AH, et al. Demyelination increases radial diffusivity in corpus callosum of mouse brain. NeuroImage. 2005;26(1):132–40. [PubMed: 15862213]
82. Bartzokis G, Lu PH, Tingus K, Mendez MF, Richard A, Peters DG, et al. Lifespan trajectory of myelin integrity and maximum motor speed. Neurobiol Aging. 2010;31(9):1554–62. [PubMed: 18926601]
83. Alonso-Ortiz E, Levesque IR, Pike GB. MRI-based myelin water imaging: A technical review. Magnetic resonance in medicine. 2015;73(1):70–81. [PubMed: 24604728]
84. Does MD. Inferring brain tissue composition and microstructure via MR relaxometry. NeuroImage. 2018;182:136–48. [PubMed: 29305163]

85. Paternoster R, Brame R, Mazerolle P, Piquero A. USING THE CORRECT STATISTICAL TEST FOR THE EQUALITY OF REGRESSION COEFFICIENTS Criminology. 1998;36:859–66.

86. Benjamini Y Discovering the false discovery rate. Journal of the Royal Statistical Society Series B (Statistical Methodology). 2010;72(4):405–16.

87. Benjamini Y, Hochberg Y. Controlling the False Discovery Rate: A Practical and Powerful Approach to Multiple Testing. Journal of the Royal Statistical Society Series B (Methodological). 1995;57(1):289–300.

88. Inano S, Takao H, Hayashi N, Abe O, Ohtomo K. Effects of age and gender on white matter integrity. AJNR American journal of neuroradiology. 2011;32(11):2103–9. [PubMed: 21998104]

89. Sullivan EV, Pfefferbaum A. Diffusion tensor imaging and aging. Neuroscience & Biobehavioral Reviews. 2006;30(6):749–61. [PubMed: 16887187]

90. Saito N, Sakai O, Ozonoff A, Jara H. Relaxo-volumetric multispectral quantitative magnetic resonance imaging of the brain over the human lifespan: global and regional aging patterns. Magnetic resonance imaging. 2009;27(7):895–906. [PubMed: 19520539]

91. Mädler B, Drabycz SA, Kolind SH, Whittall KP, MacKay AL. Is diffusion anisotropy an accurate monitor of myelination? Correlation of multicomponent T2 relaxation and diffusion tensor anisotropy in human brain. Magn Reson Imaging. 2008;26(7):874–88. [PubMed: 18524521]

92. Alexander AL, Lee JE, Lazar M, Field AS. Diffusion tensor imaging of the brain. Neurotherapeutics. 2007;4(3):316–29. [PubMed: 17599699]

93. Alexander AL, Hurley SA, Samsonov AA, Adluru N, Hosseinbor AP, Mossahebi P, et al. Characterization of Cerebral White Matter Properties Using Quantitative Magnetic Resonance Imaging Stains. Brain Connect. 2011;1(6):423–46. [PubMed: 22432902]

94. Feldman HM, Yeatman JD, Lee ES, Barde LHF, Gaman-Bean S. Diffusion Tensor Imaging: A Review for Pediatric Researchers and Clinicians. J Dev Behav Pediatr. 2010;31(4):346–56. [PubMed: 20453582]

95. Stricker NH, Schweinsburg BC, Delano-Wood L, Wierenga CE, Bangen KJ, Haaland KY, et al. Decreased white matter integrity in late-myelinating fiber pathways in Alzheimer's disease supports retrogenesis. NeuroImage. 2009;45(1):10–6. [PubMed: 19100839]

96. Bender AR, Völkle MC, Raz N. Differential aging of cerebral white matter in middle-aged and older adults: A seven-year follow-up. NeuroImage. 2016;125:74–83. [PubMed: 26481675]

97. Bouhrara M, Kim RW, Khattar N, Qian W, Bergeron CM, Melvin D, et al. Age-related estimates of aggregate g-ratio of white matter structures assessed using quantitative magnetic resonance neuroimaging. Human brain mapping.n/a(n/a).

98. Yeatman JD, Wandell BA, Mezer AA. Lifespan maturation and degeneration of human brain white matter. Nat Commun. 2014;5:4932. [PubMed: 25230200]

99. Fjell AM, Walhovd KB, Westlye LT, Ostby Y, Tamnes CK, Jernigan TL, et al. When does brain aging accelerate? Dangers of quadratic fits in cross-sectional studies. NeuroImage. 2010;50(4):1376–83. [PubMed: 20109562]

100. West DJ, Teixeira RPAG, Wood TC, Hajnal JV, Tournier J-D, Malik SJ. Inherent and unpredictable bias in multi-component DESPOT myelin water fraction estimation. NeuroImage. 2019;195:78–88. [PubMed: 30930311]

101. Kalantari S, Laule C, Bjarnason TA, Vavasour IM, MacKay AL. Insight into in vivo magnetization exchange in human white matter regions. Magnetic resonance in medicine. 2011;66(4):1142–51. [PubMed: 21381107]

102. Myint W, Ishima R. Chemical exchange effects during refocusing pulses in constant-time CPMG relaxation dispersion experiments. Journal of biomolecular NMR. 2009;45(1–2):207–16. [PubMed: 19618276]

103. Zhang J, Kolind SH, Laule C, MacKay AL. How does magnetization transfer influence mcDESPOT results? Magnetic resonance in medicine. 2015;74(5):1327–35. [PubMed: 25399771]

104. Birkl C, Birkl-Toeglhofer AM, Endmayr V, Hoftberger R, Kasprian G, Krebs C, et al. The influence of brain iron on myelin water imaging. NeuroImage. 2019;199:545–52. [PubMed: 31108214]

105. Washburn KE, Eccles CD, Callaghan PT. The dependence on magnetic field strength of correlated internal gradient relaxation time distributions in heterogeneous materials. Journal of magnetic resonance (San Diego, Calif : 1997). 2008;194(1):33–40.

106. Seland JG, Washburn KE, Anthonsen HW, Krane J. Correlations between diffusion, internal magnetic field gradients, and transverse relaxation in porous systems containing oil and water. Physical review E, Statistical, nonlinear, and soft matter physics. 2004;70(5 Pt 1):051305.

107. Ziener CH, Kampf T, Jakob PM, Bauer WR. Diffusion effects on the CPMG relaxation rate in a dipolar field. Journal of magnetic resonance (San Diego, Calif : 1997). 2010;202(1):38–42.

108. Carney CE, Wong ST, Patz S. Analytical solution and verification of diffusion effect in SSFP. Magnetic resonance in medicine. 1991;19(2):240–6. [PubMed: 1881310]

109. Le Bihan D, Turner R, MacFall JR. Effects of intravoxel incoherent motions (IVIM) in steady-state free precession (SSFP) imaging: application to molecular diffusion imaging. Magnetic resonance in medicine. 1989;10(3):324–37. [PubMed: 2733589]

110. Piredda GF, Hilbert T, Thiran J-P, Kober T. Probing myelin content of the human brain with MRI: A review. Magnetic resonance in medicine.n/a(n/a).

111. Heath F, Hurley SA, Johansen-Berg H, Sampaio-Baptista C. Advances in noninvasive myelin imaging. Developmental neurobiology. 2018;78(2):136–51. [PubMed: 29082667]

112. Lazari A, Lipp I. Can MRI measure myelin? Systematic review, qualitative assessment, and meta-analysis of studies validating microstructural imaging with myelin histology. NeuroImage. 2021:117744. [PubMed: 33524576]

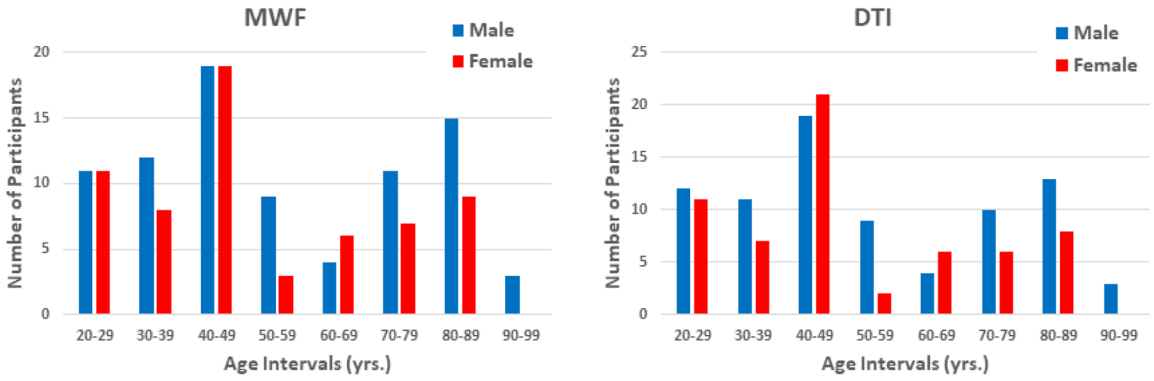

Figure 1.
Number of participants per age decade and sex within the study cohort for MWF and DTI.

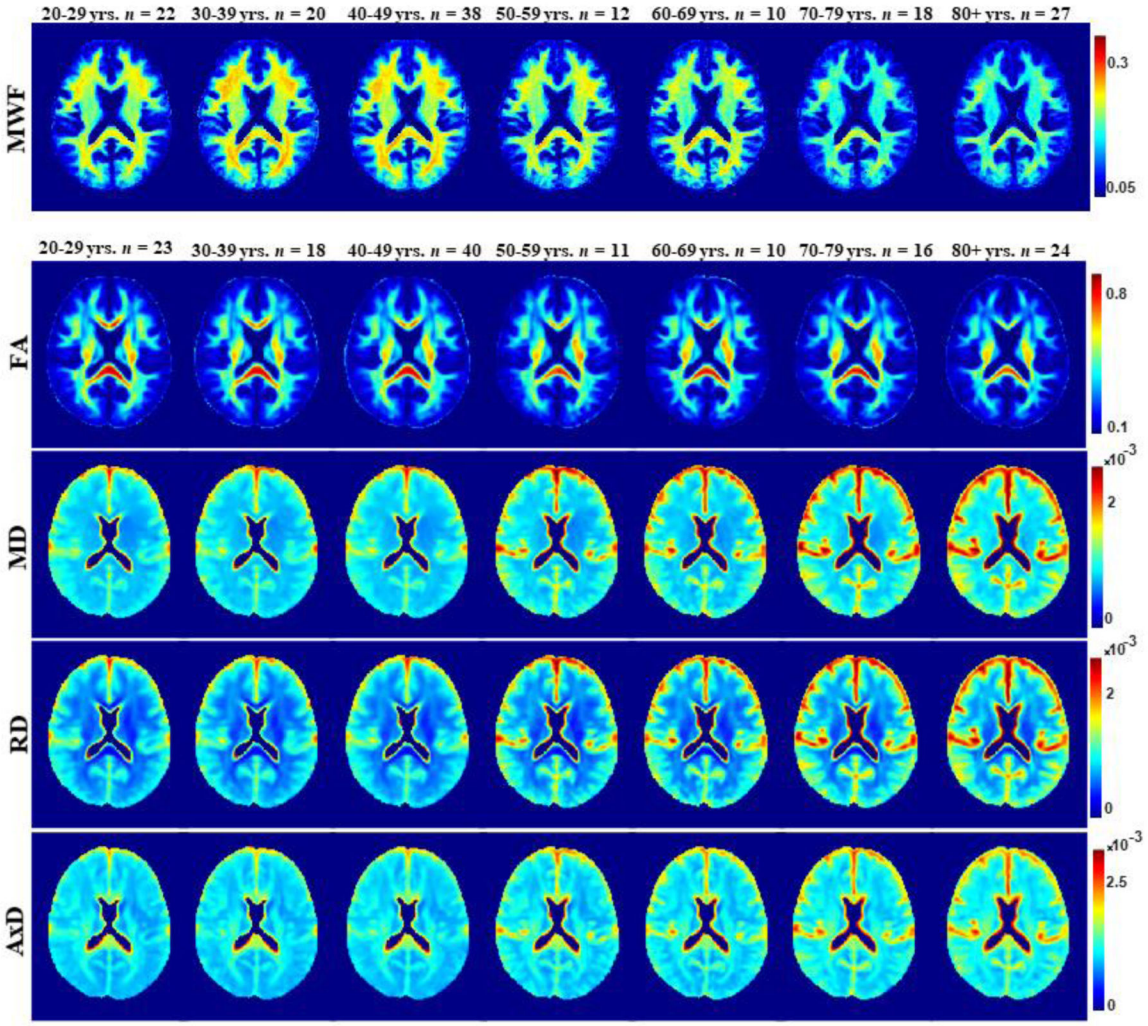

Figure 2.

MWF, FA, MD, RD, and AxD represented as averaged participant maps calculated across age decades. The displayed parameter maps correspond to slice number 90 of the MNI atlas. Visual inspection indicates an increase in MWF values from early adulthood to middle age, followed by a decrease in values afterwards. FA, MD, RD, and AxD show earlier peaks in early adulthood, with lower FA values and higher MD, RD, and AxD values at advanced age.

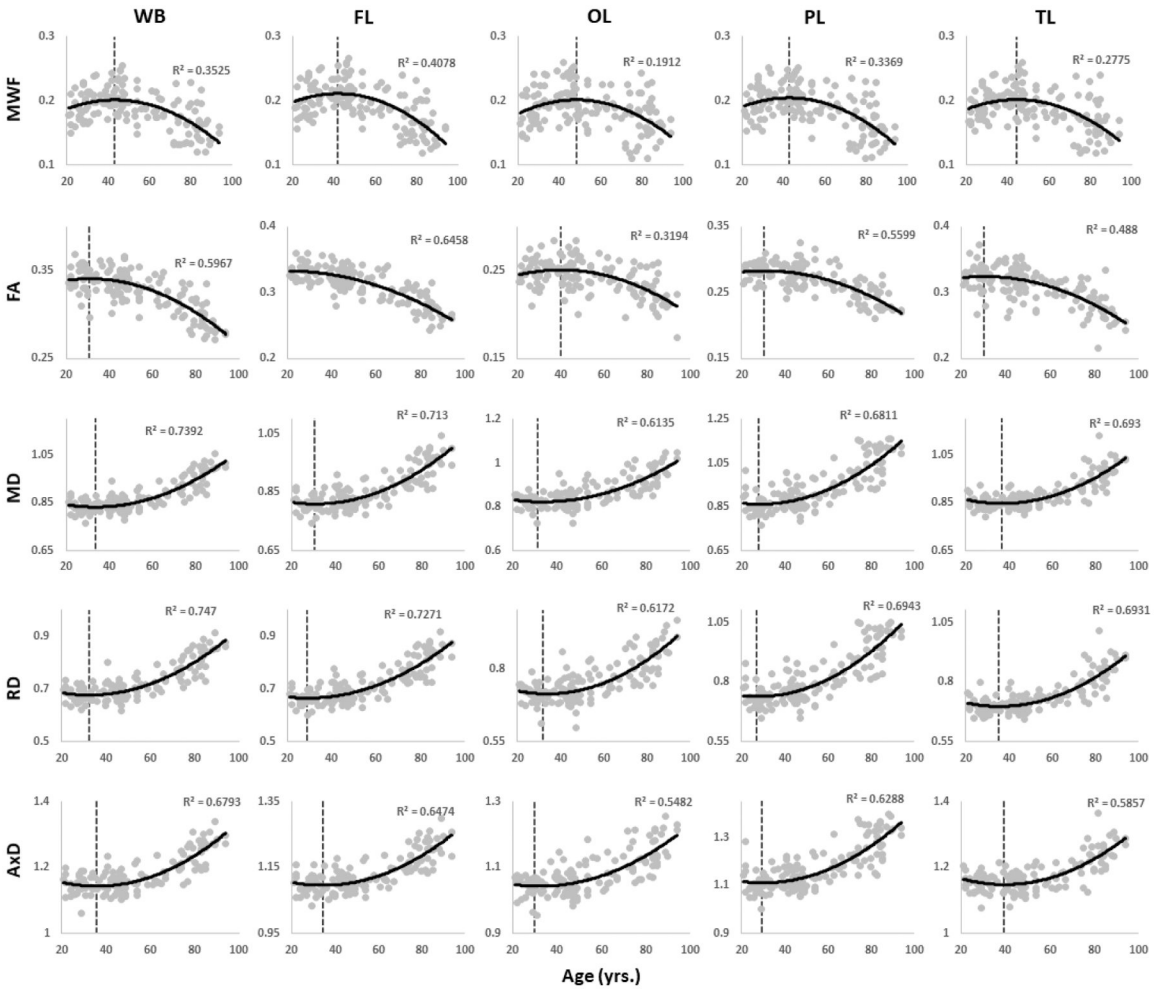

Figure 3.

Plots illustrating regional MWF, FA, MD, RD, or AxD values as a function of age for five representative cerebral white matter ROIs: whole brain (WB) WM, frontal (FL), occipital (OL), parietal (PL), and temporal (TL) lobes WM. For each ROI, the coefficient of determination, R^2, is reported. Plots of all ROIs can be found in the Supplementary Material (Figs. S1–S5).

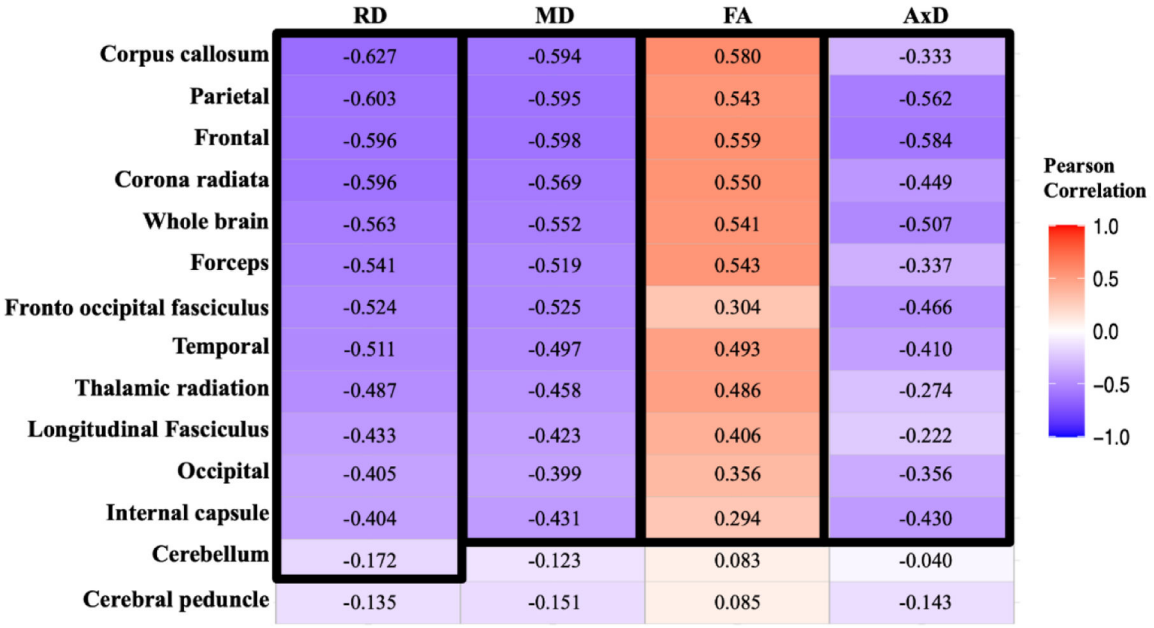

Figure 4.

Correlational matrix providing the Pearson correlation coefficient, R^2, of each DTI metric vs. MWF for each ROI. Cell values in a black box represent the Pearson correlation coefficients that were statistically significant after FDR ($p < 0.05$). The ROIs are ranked in order of decreasing mean R^2 values across all metrics. Similarly, the MR parameters themselves are ranked in descending order of mean R^2 values across all ROIs.

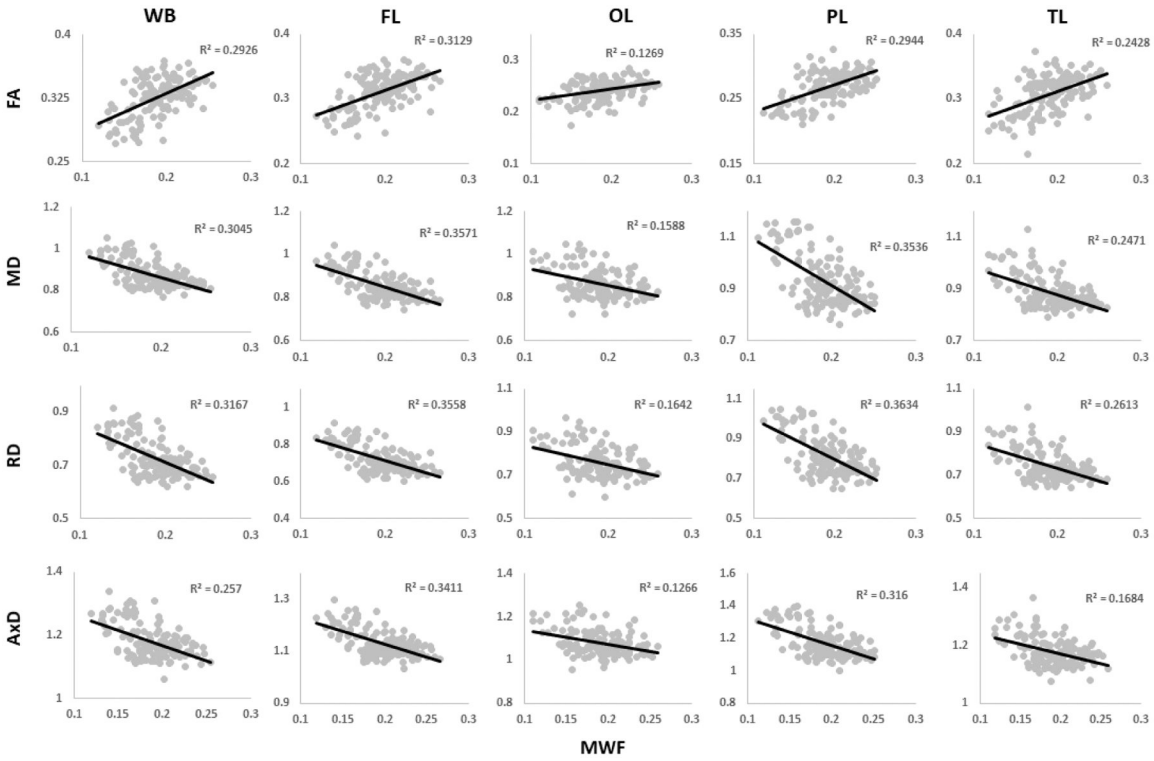

Figure 5.

Plots illustrating regional Pearson correlations between FA, MD, RD, or AxD and MWF for five representative cerebral white matter ROIs corresponding to the whole brain (WB) WM, frontal (FL), occipital (OL), parietal (PL), and temporal (TL) lobes WM. For each ROI, the coefficient of determination, R^2, is reported. Plots of all ROIs can be found in the Supplementary Material (Figs. S6–S9).

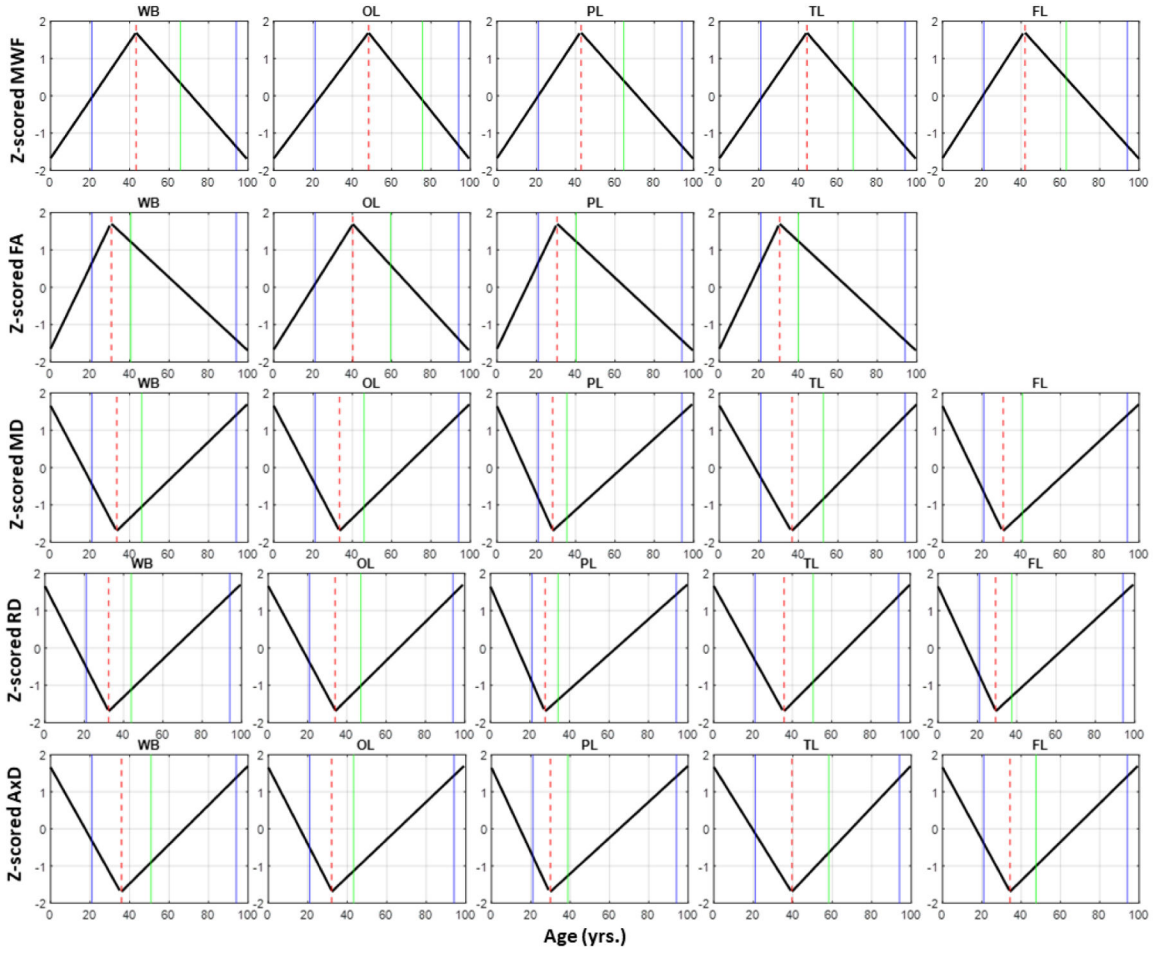

Figure 6.

Plots illustrating the piecewise linear fits of the maturation and degeneration phases as a function of age for all MR parameters and 5 representative ROIs: whole brain (WB) WM, frontal (FL), occipital (OL), parietal (PL), and temporal (TL) lobes WM. The blue solid lines indicate the actual age range of our cohort, the dashed red line indicates the peak ages, while the green line indicates the age at a symmetrical age interval between the minimum age of our cohort and the peak. Plots of all ROIs can be found in the Supplementary Material (Figs. S10–S14).

Table 1.

Cohort characteristics for each MR modality.

	Age (yrs.)		Sex	
	Range	**Mean ± SD**	**Men**	**Women**
MWF	21 – 94	53.7 ± 21.1	84	63
DTI	21 – 94	52.7 ± 21.3	81	61

SD: standard deviation, MWF: myelin water fraction, DTI: diffusion tensor imaging. For each modality, age was not significantly different between men and women.

Table 2.

Regression coefficient ± standard error of age and age^2 terms incorporated in the linear regression for the 14 cerebral white matter structures and for each MR parameter studied. Sex results were not reported as it exhibited nonsignificant effect.

	MWF		FA		MD		RD		AxD	
	Age ($\times 10^{-3}$)	**Age^2 ($\times 10^{-5}$)**	**Age ($\times 10^{-3}$)**	**Age^2 ($\times 10^{-5}$)**	**Age ($\times 10^{-6}$)**	**Age^2 ($\times 10^{-8}$)**	**Age ($\times 10^{-6}$)**	**Age^2 ($\times 10^{-8}$)**	**Age ($\times 10^{-6}$)**	**Age^2 ($\times 10^{-8}$)**
Whole Brain	2.33±0.63 *	−2.66±0.55 *	0.98±0.39 *	−1.59±0.34 *	−3.50±0.84 *	5.25±0.74 *	−3.52±0.89 *	5.46±0.78 *	−3.41±0.80 *	4.75±0.70 *
Frontal	2.45±0.66 *	−2.90±0.58 *	0.52±0.41 *	−1.33±0.36 *	−2.90±0.89 *	4.73±0.78 *	−2.87±0.95 *	4.95±0.84 *	−2.92±0.82 *	4.27±0.72 *
Occipital	2.77±0.76 *	−2.85±0.67 *	1.13±0.43 *	−1.42±0.37 *	−3.09±1.02 *	4.74±0.89 *	−3.44±1.08 *	5.18±0.95 *	−2.34±0.99 *	3.79±0.87 *
Parietal	2.44±0.69 *	−2.81±0.61 *	0.94±0.42 *	−1.56±0.37 *	−3.63±1.45 *	6.51±1.27 *	−3.67±1.49 *	6.73±1.31 *	−3.60±1.44 *	6.07±1.26 *
Temporal	2.38±0.70 *	−2.65±0.62 *	1.05±0.53 *	−1.73±0.47 *	−4.11±0.89 *	5.63±0.78 *	−4.31±1.00 *	6.08±0.88 *	−3.66±0.82 *	4.65±0.72 *
Cerebellum	1.80±0.68 *	−1.94±0.60 *	1.60±0.63	−1.56±0.56 *	−2.93±1.03 *	2.89±0.90 *	−3.07±1.07 *	3.04±0.94 *	−2.60±1.21	2.52±1.06 *
Corpus Callosum	1.87±0.64 *	−2.31±0.57 *	0.94±1.18 *	−2.55±1.04 *	−2.24±1.85 *	5.39±1.63 *	−2.15±2.29 *	6.08±2.01 *	−2.73±1.75 *	4.21±1.54 *
Internal Capsule	1.97±0.64 *	−2.37±0.56 *	2.74±0.88 *	−2.86±0.77 *	−5.37±1.13 *	6.20±0.99 *	−4.84±1.18 *	5.62±1.03 *	−6.50±1.34 *	7.38±1.17 *
Cerebral Peduncle	2.00±0.59	−1.93±0.52 *	−0.62±0.82 *	−0.063±0.72	−2.78±1.28 *	3.97±1.12 *	−1.79±1.28 *	3.23±1.13 *	−4.69±1.67 *	5.28±1.47 *
Corona Radiata	2.43±0.79 *	−3.03±0.70 *	1.09±0.62 *	−1.83±0.54 *	−2.71±1.03 *	4.17±0.90 *	−2.78±1.09 *	4.40±0.95 *	−2.50±1.09 *	3.61±0.96 *
Thalamic Radiation	1.68±0.71 *	−2.22±0.63 *	1.51±0.58 *	−2.10±0.51 *	−2.82±0.93 *	3.91±0.81 *	−3.16±1.00 *	4.41±0.87 *	−1.84±0.94 *	2.59±0.83 *
Fronto Occipital Fasciculus	2.21±0.69 *	−2.70±0.61 *	1.24±0.71 *	−1.54±0.62 *	−3.46±1.02 *	4.78±0.90 *	−3.68±1.09 *	4.94±0.96 *	−3.08±1.13 *	4.47±1.00 *
Longitudinal Fasciculus	2.19±0.70 *	−2.60±0.62 *	0.63±0.71 *	−1.16±0.62	−2.51±0.74 *	3.26±0.65 *	−2.53±0.86 *	3.45±0.76 *	−2.33±0.91 *	2.70±0.80 *
Forceps	2.21±0.70 *	−2.64±0.61 *	1.32±0.65 *	−2.34±0.57 *	−3.07±0.89 *	4.71±0.78 *	−3.45±1.04 *	5.51±0.91 *	−2.31±0.91 *	3.06±0.80 *

* indicates significance at $p < 0.05$ after FDR correction. The actual p-values are provided in the Supplementary Material (Table S1).

Table 3.

Likelihood-ratio test p-values comparing regression models to assess whether the data supports a quadratic model versus a linear model for all metrics in all ROIs. Bold indicates significance at $p < 0.05$.

	MWF	FA	MD	RD	AxD
Whole Brain	**1.91×10^{-5}**	**6.10×10^{-5}**	**1.86×10^{-10}**	**5.24×10^{-10}**	**2.40×10^{-9}**
Frontal	**1.74×10^{-5}**	**4.43×10^{-4}**	**2.32×10^{-8}**	**5.41×10^{-8}**	**5.41×10^{-8}**
Occipital	**4.64×10^{-5}**	**4.43×10^{-4}**	**5.90×10^{-7}**	**3.72×10^{-7}**	**4.02×10^{-5}**
Parietal	**3.09×10^{-5}**	**1.77×10^{-4}**	**1.26×10^{-6}**	**1.00×10^{-6}**	**7.46×10^{-6}**
Temporal	**4.64×10^{-5}**	**4.43×10^{-4}**	**1.86×10^{-10}**	**5.24×10^{-10}**	**6.45×10^{-9}**
Cerebellum	**1.25×10^{-3}**	**7.24×10^{-3}**	**1.38×10^{-3}**	**1.54×10^{-3}**	**0.0167**
Corpus Callosum	**7.63×10^{-5}**	**0.0161**	**1.05×10^{-3}**	**2.79×10^{-3}**	**6.69×10^{-3}**
Internal Capsule	**4.64×10^{-5}**	**4.43×10^{-4}**	**1.38×10^{-8}**	**3.72×10^{-7}**	**1.03×10^{-8}**
Cerebral Peduncle	**3.09×10^{-4}**	0.929	**5.10×10^{-4}**	**4.20×10^{-3}**	**4.89×10^{-4}**
Corona Radiata	**4.64×10^{-5}**	**1.20×10^{-3}**	**7.83×10^{-6}**	**9.31×10^{-6}**	**2.99×10^{-4}**
Thalamic Radiation	**4.81×10^{-4}**	**1.77×10^{-4}**	**3.65×10^{-6}**	**1.47×10^{-6}**	**2.09×10^{-3}**
Fronto Occipital Fasciculus	**4.64×10^{-5}**	**0.0161**	**5.90×10^{-7}**	**1.00×10^{-6}**	**2.48×10^{-5}**
Longitudinal Fasciculus	**4.64×10^{-5}**	0.0630	**1.77×10^{-6}**	**1.00×10^{-5}**	**9.61×10^{-4}**
Forceps	**4.64×10^{-5}**	**1.77×10^{-4}**	**2.32×10^{-8}**	**3.50×10^{-8}**	**2.48×10^{-4}**

Table 4.

Table of peak ages (in years) for each MR parameters in the 14 cerebral white matter ROIs investigated. NS indicates that the quadratic effect of age, age^2, was not significant, while NA indicates that the calculated peak age was outside of the sample age range.

	MWF	FA	MD	RD	AxD
Whole Brain	43.76	30.86	33.40	32.28	35.84
Frontal	42.34	NA	30.68	28.98	34.20
Occipital	48.58	40.07	31.48	32.09	29.91
Parietal	43.34	30.27	27.92	27.24	29.69
Temporal	44.83	30.35	36.55	35.48	39.37
Cerebellum	46.34	51.32	51.01	50.84	51.71
Corpus Callosum	40.51	NA	NA	NA	32.58
Internal Capsule	41.41	47.77	43.32	43.07	43.98
Cerebral Peduncle	51.70	NS	34.27	26.24	44.18
Corona Radiata	40.16	29.76	32.48	31.58	34.55
Thalamic Radiation	37.84	35.84	35.46	35.48	35.51
Fronto Occipital Fasciculus	40.88	40.12	36.23	37.26	34.47
Longitudinal Fasciculus	42.21	NS	38.32	36.59	43.09
Forceps	41.86	28.18	33.26	31.85	38.60

Table 5.

The slopes ± standard error of the maturation (Mat) and degeneration (Deg) phases of the standardized MWF and DTI indices for the 14 white matter ROIs investigated. All maturation and degeneration rates were statistically compared, with none being significantly different. NA indicates that maturation/degeneration rates could not be calculated, see Table 4.

	MWF		FA		MD		RD		AxD	
	Mat Rate ($\times 10^{-3}$)	Deg Rate ($\times 10^{-3}$)	Mat Rate ($\times 10^{-3}$)	Deg Rate ($\times 10^{-3}$)	Mat Rate ($\times 10^{-6}$)	Deg Rate ($\times 10^{-6}$)	Mat Rate ($\times 10^{-6}$)	Deg Rate ($\times 10^{-6}$)	Mat Rate ($\times 10^{-6}$)	Deg Rate ($\times 10^{-6}$)
Whole Brain	1.16±0.46	−1.25±0.13	0.95±1.07	−0.91±0.08	−3.02±1.85	2.94±0.19	−3.76±2.29	3.14±0.20	−1.89±1.50	2.48±0.19
Frontal	1.30±0.59	−1.40±0.12	NA	NA	−3.98±2.53	2.80±0.19	−5.38±3.16	3.02±0.20	−2.22±1.60	2.34±0.19
Occipital	1.05±0.36	−1.18±0.25	0.45±0.47	−0.67±0.10	−3.31±2.24	2.83±0.24	−3.39±2.15	3.04±0.25	−3.05±2.54	2.34±0.22
Parietal	1.18±0.57	−1.31±0.14	1.72±1.14	−0.95±0.09	−12.36±5.48	4.17±0.28	−14.47±7.58	4.37±0.27	−7.91±4.56	3.75±0.28
Temporal	1.18±0.47	−1.24±0.16	1.22±1.46	−1.01±0.11	−2.44±1.58	2.98±0.21	−2.94±1.88	3.30±0.24	−1.54±1.10	2.27±0.20
Cerebellum	0.92±0.41	−0.89±0.16	0.57±0.31	−0.62±0.27	−0.83±0.51	1.02±0.45	−0.90±0.53	1.09±0.47	−0.71±0.60	0.86±0.52
Corpus Callosum	1.12±0.66	−1.19±0.12	NA	NA	NA	NA	NA	NA	−3.5±6.91	4.93±0.60
Internal Capsule	1.25±0.64	−1.19±0.11	0.60±0.49	−0.99±0.31	−1.19±0.97	2.50±0.31	−0.96±1.00	2.24±0.32	−1.69±1.02	3.02±0.38
Cerebral Peduncle	0.71±0.26	−0.79±0.22	NA	NA	−1.57±2.28	2.10±0.29	−1.41±6.47	1.93±0.23	−1.27±1.24	2.19±0.46
Corona Radiata	1.61±0.92	−1.52±0.15	1.14±1.96	−1.05±0.12	−2.41±2.53	2.35±0.22	−2.98±2.68	2.52±0.23	−1.25±2.08	1.93±0.25
Thalamic Radiation	1.99±1.06	−1.25±0.13	0.75±1.05	−1.05±0.13	−1.56±1.58	2.04±0.21	−1.77±1.81	2.30±0.23	−0.81±1.59	1.36±0.22
Fronto Occipital Fasciculus	1.45±0.70	−1.35±0.12	0.26±0.92	−0.66±0.17	−1.50±1.78	2.43±0.24	−1.46±1.77	2.44±0.26	−1.29±2.19	2.34±0.26
Longitudinal Fasciculus	1.33±0.62	−1.27±0.14	NA	NA	−0.87±1.20	1.57±0.17	−1.13±1.48	1.76±0.20	−0.53±0.77	1.13±0.24
Forceps	1.28±0.63	−1.30±0.14	1.78±2.48	−1.42±0.13	−2.40±2.29	2.66±0.20	−3.39±2.68	3.20±0.23	−0.77±1.45	1.50±0.21